ESI

Boosting photocatalytic hydrogen production activity by microporous Cu^{II}-MOF nanoribbon decorated with Pt nanoparticles

Lei Li,[a, b] Yan Zhao,[a, b] Qian Wang,[a] Zheng-Yu Liu,[a] Xiu-Guang Wang,[a] En-Cui Yang,*[a] and Xiao-Jun Zhao*[a,b]

[a] *College of Chemistry, Key Laboratory of Inorganic-Organic Hybrid Functional Material Chemistry, Ministry of Education, Tianjin Key Laboratory of Structure and Performance for Functional Molecules, Tianjin Normal University, Tianjin 300387, People's Republic of China*

[b] *Department of Chemistry, Collaborative Innovation Center of Chemical Science and Engineering, Nankai University, Tianjin 300071, People's Republic of China*

Materials and characterizations

All raw materials were commercially purchased from either J&K Scientific or Tianjin Chemical Reagent Factory and used as received without further purification. Doubly deionized water was used during the conventional synthesis. HL was prepared according to the literature.[1] Elemental analyses for C, H and N were carried out with a CE–440 (Leeman–Labs) analyzer. Fourier transform (FT) IR spectra (KBr pellets) were taken on an Avatar–370 (Nicolet) spectrometer in the range 4000–400 cm^{-1}. Thermogravimetric analysis (TGA) experiments were performed on a Shimadzu simultaneous DTG–60A compositional analysis instrument from room temperature to 800 ^{o}C under N_2 atmosphere at a heating rate of 5 ^{o}C min^{-1}. Powder X-ray diffraction (PXRD) patterns were obtained from a Bruker D8 ADVANCE diffractometer at 40 kV and 40 mA for Cu $K\alpha$ radiation (λ = 1.5406 Å), with a scan speed of 0.1 sec/step and a step size of 0.01^{o} in 2θ. The simulated PXRD pattern was calculated using single-crystal X-ray diffraction data and

processed by the free Mercury v1.4 program provided by the Cambridge Crystallographic Data Center. The X-ray photoelectron spectroscopy (XPS) measurement was carried out on an AXIS Ultra DLD X-ray photoelectron spectroscopy (Shimadzu, Japan). The scanning electron microscope (SEM) characterizations were performed by a field-emission scanning electron microscope (SEM, FEI NOVA Nano SEM 230) with energy dispersive spectroscope (EDS). UV-vis diffuse reflectance spectra (DRS) were carried out on a U-4100 UV-vis spectrophotometer (HITACHI) equipped with an integrating sphere assembly. Fluorescence spectra were recorded in aqueous solution with a Cary Eclipse fluorescence spectrophotometer (Varian) at room temperature. Electron spin resonance (ESR) spectra were measured in tert-butanol with EDTA as trapping agent on an electron paramagnetic resonance spectrometer (ER200-SRC-10/12). The weight percentage of Pt in the resulting product was determined by inductively coupled plasma mass spectrometter (ICP-MS, iCAP RQ). Transmission electron microscopy (TEM) images, high-resolution transmission electron microscopy (HRTEM) and EDS elemental mapping were obtained by a TecnaiG2 F20 transmission electron microscopy at 200 kV. The Mott-Schottky plots were measured in 0.2 M Na_2SO_4 aqueous solution (pH = 10) adjusted by NaOH (1.0 M) aqueous solution with an AMETEK Princeton Applied Research (Versa STAT 4) electrochemical workstation using photocatalyst/FTO combination as the working electrode, a platinum foil as the counter electrode, and a saturated Ag/AgCl as the reference electrode. The working electrode photocatalyst/FTO was prepared by dropping 50 μL of sample suspension containing containing photocatalyst (3.0 mg), ethanol (1.0 mL) and Nafion (20.0 μL) directly onto a FTO plate. The surface area of the working electrode exposed to the electrolyte was about 1.0 cm^2. The electrochemical impedance spectroscopy (EIS) of crystalline Cu^{II}-MOF and Pt/Cu^{II}-MOF composites were carried out in 0.2 M Na_2SO_4 aqueous solution (pH = 10) with a bias of 2.0 V.

Table S1 Crystal and structure refinement data for **Cu^{II}-MOF** [a]

	Cu^{II}-MOF[2]
empirical formula	$C_{29}H_{19}CuN_3O_5$
F_w	553.01
cryst size [mm]	0.22 × 0.21 × 0.18
cryst syst	Orthorhombic
space group	$P2_12_12_1$
a [Å]	6.2062(4)
b [Å]	19.1198(12)
c [Å]	25.5158(17)
V [Å^3]	3027.7(3)
Z, D_c [g cm^{-3}]	4, 1.213
h / k / l	– 5, 7 / – 24, 22 / – 30, 32
F(000)	1132
μ [mm^{-1}]	0.759
reflections collected/ unique	19906 / 6280
R_{int}	0.0439
data / restraints / params	6280 / 0 / 344
R_1 [a], wR_2 [b] [$I > 2\sigma(I)$]	0.0397, 0.0920
R_1, wR_2 [all data]	0.0449, 0.0948
Max. and min. transmission	0.875 and 0.851
GOF on F^2	1.050
$\Delta\rho_{max}$, $\Delta\rho_{min}$ [e•Å^{-3}]	0.374 / – 0.348

[a] $R_1 = \Sigma(||F_o|-|F_c||)/\Sigma|F_o|$; [b] $wR_2 = [\Sigma w(|F_o|^2-|F_c|^2)^2/\Sigma w(F_o^2)^2]^{1/2}$.

Table S2 Selected bond lengths (Å) and angles (deg) for **Cu^{II}-MOF** [a]

Cu(1)–O(1)	1.996(3)	Cu(1)–N(1)	2.021(3)
Cu(1)–O(4)$^{\#1}$	1.918(2)	Cu(1)–N(3)$^{\#2}$	1.999(3)
Cu(1)–O(2)	2.407(3)		
O(4)$^{\#1}$–Cu(1)–N(3)$^{\#2}$	93.22(12)	O(1)–Cu(1)–N(3)$^{\#2}$	91.71(12)
O(4)$^{\#1}$–Cu(1)–N(1)	91.70(12)	O(1)–Cu(1)–N(1)	87.49(13)
O(4)$^{\#1}$–Cu(1)–O(2)	105.80(11)	O(1)–Cu(1)–O(2)	58.72(11)
N(3)$^{\#2}$–Cu(1)–O(2)	100.93(14)	N(1)–Cu(1)–O(2)	92.15(14)

[a] Symmetry codes: $^{\#1}$ − *x*, *y* − 1/2, 3/2 − *z*, $^{\#2}$ 1/2− *x*, 1 − *y*, *z* + 1/2.

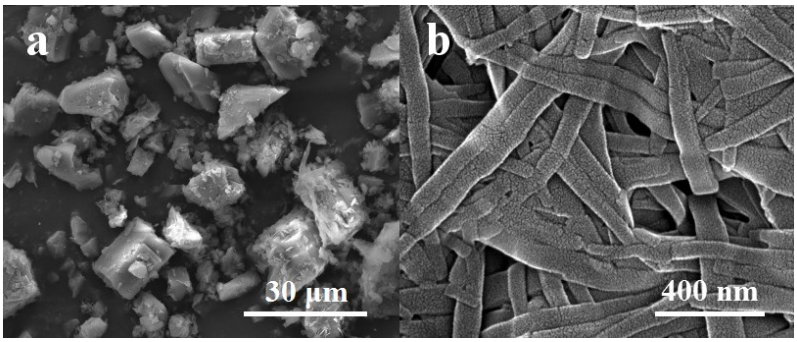

Fig. S1. (a) SEM image of **Cu^{II}-MOF** obtained from mixed H_2O-CH_3OH solution. (b) SEM image of **Cu^{II}-MOF** obtained from acidic H_2O-CH_3OH solution adjusted by 1.0 M HCl aqueous solution (pH = 3.28).

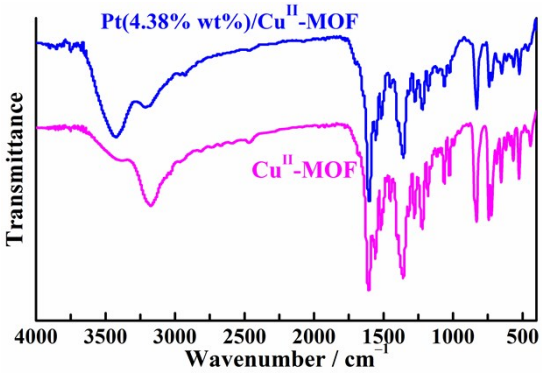

Fig. S2. FT-IR spectra of **Cu^{II}-MOF** and **Pt(4.38 wt%)/Cu^{II}-MOF**.

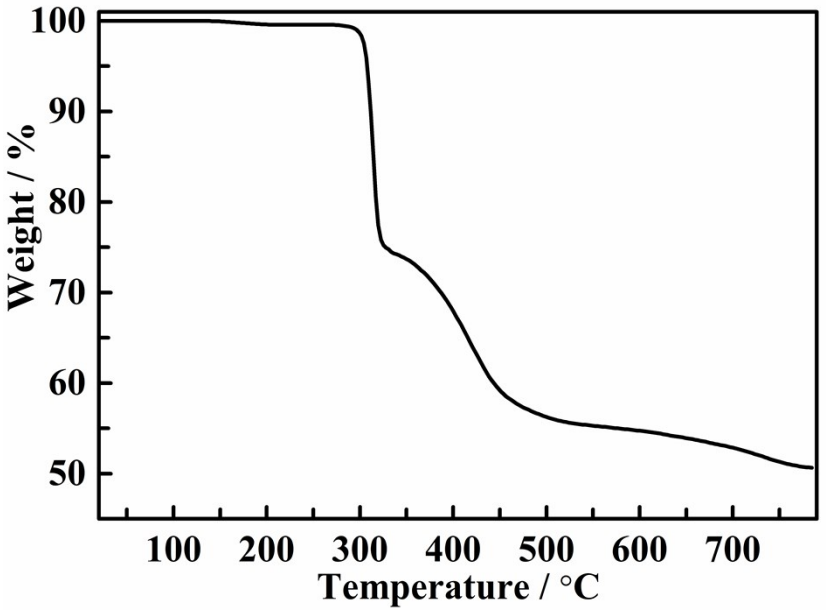

Fig. S3. TG curve for **Cu^{II}-MOF**.

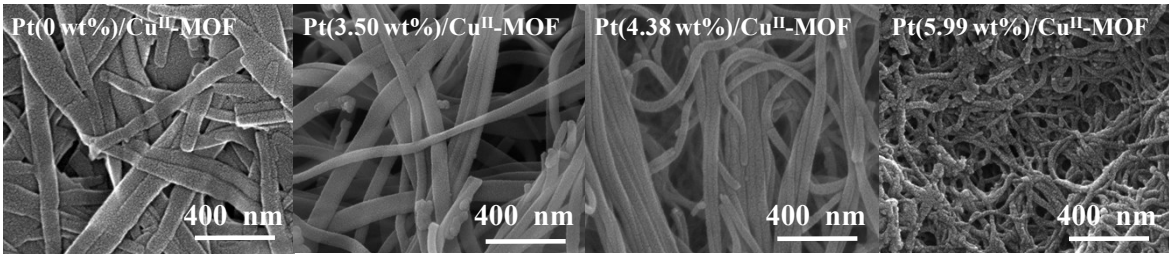

Fig. S4. SEM images of **Pt/Cu^{II}-MOF** composites with different Pt loadings.

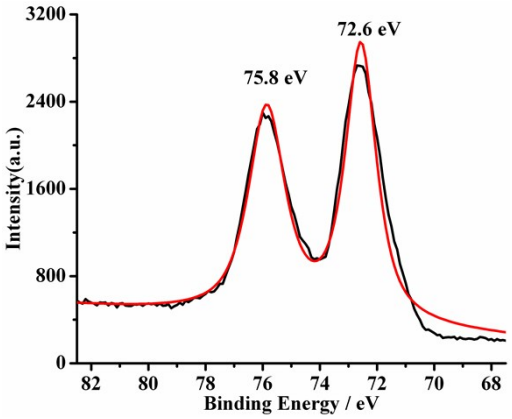

Fig. S5. Pt 4f XPS spectrum for **Pt(4.38 wt%)/Cu^{II}-MOF**.

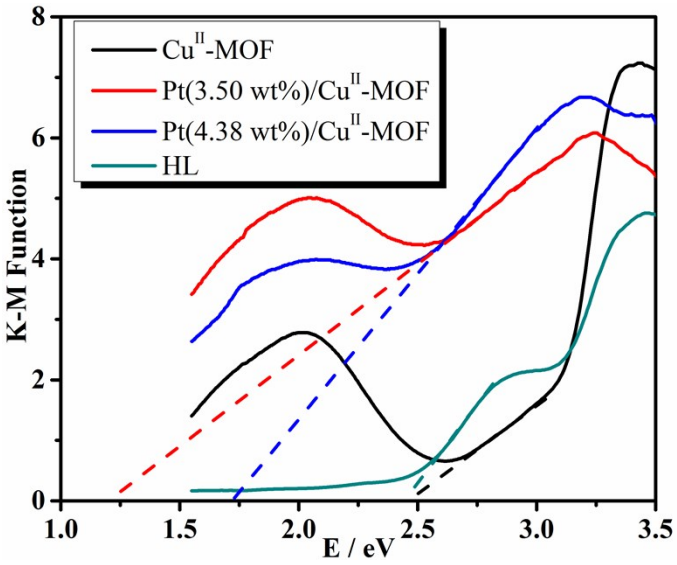

Fig. S6. Plots of K-M function vs. energy for **Cu^{II}-MOF, Pt/Cu^{II}-MOF** composites and HL ligand.

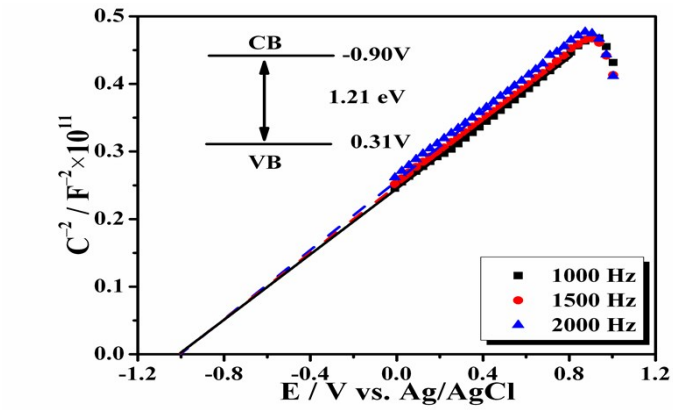

Fig. S7. Mott-Schottky plot of **Pt(3.50 wt%)/Cu^{II}-MOF** in 0.2 M Na_2SO_4 aqueous solution with pH = 10 (Inset: energy band alignment diagram for **Pt(3.50 wt%)/Cu^{II}-MOF**).

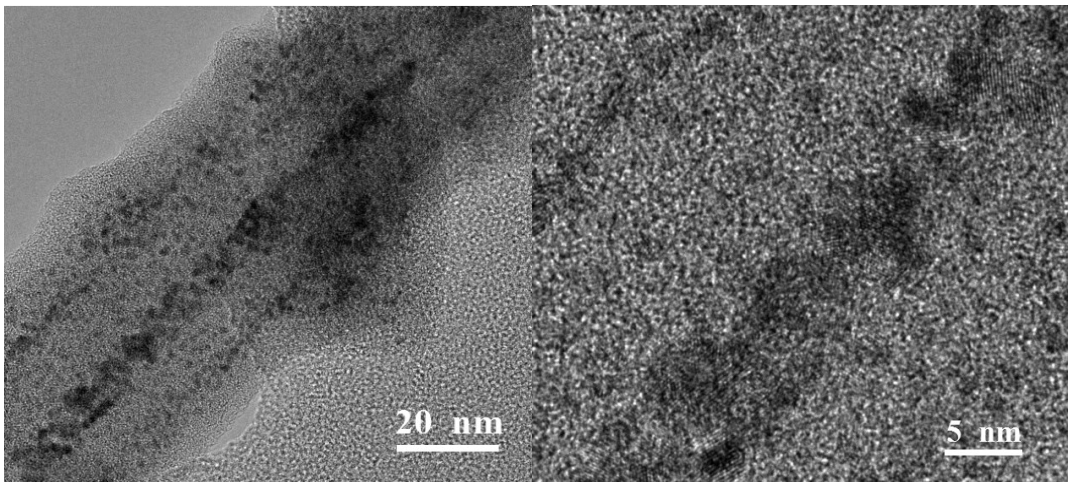

Fig. S8. HR-TEM images of **Pt(5.99 wt%)/Cu^{II}-MOF** after photocatalysis.

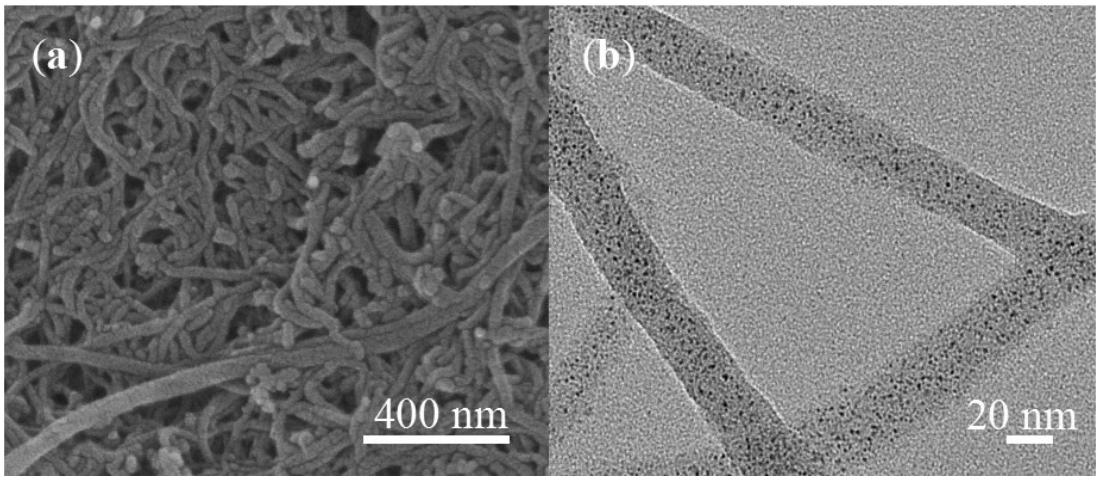

Fig. S9. SEM and TEM images of **Pt(4.38 wt%)/Cu^{II}-MOF** after photocatalysis.

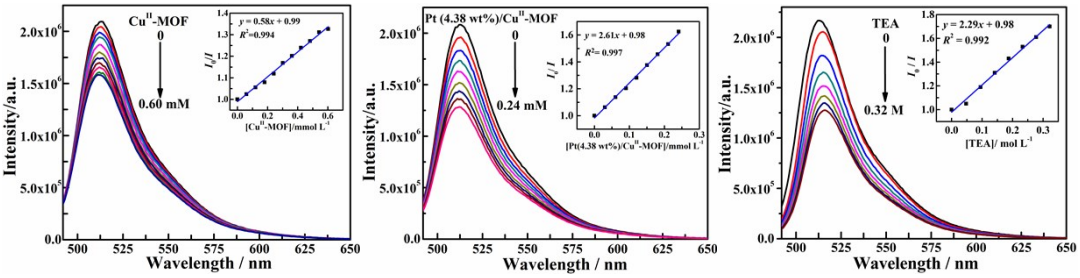

Fig. S10. Emission quenching plots of FI by **Cu^{II}-MOF** (left), **Pt(4.38 wt%)/Cu^{II}-MOF** (middle) and TEA (right) in aqueous solution (Inset: Stern-Volmer fits for the luminescence quenching of FI by **Cu^{II}-MOF**, **Pt(4.38 wt%)/Cu^{II}-MOF** and TEA).

Reference

1 Y. M. Klein, E. C. Constable, C. E. Housecroft, J. A. Zampese and A. Crochet, *CrystEngComm*, 2014, **16**, 9915–9929.

2 En-Cui Yang, CCDC 1831465: CSD communication, 2018, DOI: 10.5517/ccdc.csd.cc1zgsjr.